ISSN (Print) 1226-1750
ISSN (Online) 2233-6656
Journal of Magnetics 20(3), 211-214 (2015) http://dx.doi.org/10.4283/JMAG.2015.20.3.211

Structure and Magnetic Properties of Cr_2O_3/CrO_2 Nanoparticles Prepared by Reactive Laser Ablation and Oxidation under High Pressure of Oxygen

P. Z. Si[1]*, X. L. Wang[1], X. F. Xiao[1], H. J. Chen[1], X. Y. Liu[2], L. Jiang[1], J. J. Liu[2], Z. W. Jiao[1], and H. L. Ge[1]

[1]Zhejiang Key Lab of Magnetic Materials, or Department of Physics, China Jiliang University, Hangzhou 310018, China
[2]Faculty of Materials Science and Chemical Engineering, Ningbo University, Ningbo 315211, China

(Received 11 March 2015, Received in final form 5 June 2015, Accepted 22 June 2015)

Cr_2O_3 nanoparticles were prepared via one-step reactive laser ablation of Cr in oxygen. The metastable CrO_2 phase was obtained through the subsequent oxidation of Cr_2O_3 nanoparticles under O_2 with gas pressures of up to 40 MPa. The as-prepared Cr_2O_3 nanoparticles are spherical or rectangular in shape with sizes ranging from 20 nm to 50 nm. High oxygen pressure annealing is effective in producing meta-stable CrO_2 from as-dried Cr_2O_3 nanoparticles, and the Cr_2O_3 nanoparticles exhibit a weak ferromagnetic behavior with an exchange bias of up to 11 mT that can be ascribed to the interfacial exchange coupling between uncompensated surface spins and the antiferromagnetic core. The Cr_2O_3/CrO_2 nanoparticles exhibit an enhanced saturation magnetization and a reduced exchange bias with an increasing faction of CrO_2 due to the elimination of uncompensated surface spins over the Cr_2O_3 nanoparticles when exposed to a high pressure of O_2 and/or possible phase segregation that results in a smaller grain size for both Cr_2O_3 and CrO_2.

Keywords : laser ablation, nanoparticles, CrO_2, high oxygen pressure annealing, magnetic properties

1. Introduction

Cr_2O_3 nanoparticles are widely used as catalysts, pigments, and in wear resistance materials due to their unique physical and chemical properties [1, 2]. Cr_2O_3 nanoparticles have been previously prepared through several chemical and physical processes, including hydrothermal synthesis, arc discharge, microwave plasma, etc. [3-5]. These methods usually involve the use of wet chemicals or several steps that can be somewhat time-consuming. Recently, laser beams have been employed to synthesize Cr_2O_3 nanostructures, and well-dispersed nanoscale chromium oxide particles have been prepared via laser-induced solution deposition from solution with $CrCl_2$ and organic solvents [6]. α-Cr_2O_3 nanocondensates were fabricated using pulsed laser ablation in air [7], and Cr_2O_3 thin films were prepared on Cr thin film surfaces via laser photothermal oxidation and laser deposition using a Cr_2O_3 target [8, 9]. In this work, we prepared Cr_2O_3 nanoparticles by using one-step reactive laser ablation synthesis, which is a method that has recently emerged as a simple means to produce nanoparticles due to the ultra-high temperature of the laser beam [10, 11].

Antiferromagnetic materials with a small particles size tend to exhibit different magnetic properties, and a few antiferromagnetic nanoparticles, including MnO, CoO, NiO, have been reported to have weak ferromagnetic properties due to their uncompensated surface spins [12-14]. In our previous work, we investigated the weak ferromagnetic behavior of Cr and Cr_2O_3 nanoparticles prepared using an arc discharge method [4]. Meiklejohn and Bean first reported the exchange bias phenomenon in oxide-coated cobalt particles in 1956 [15]. Usually, the exchange bias phenomenon is present in interfaces between two substances with different magnetic orders, for instance, a ferro/antiferromagntic interface. This work investigated the structure of the Cr_2O_3 nanoparticles and the exchange bias in the interfaces between the antiferromagntic (AFM) Cr_2O_3 and the uncompensated surface layers.

Chromium dioxide (CrO_2) has been extensively studied as a result of its excellent ferromagnetic performance and its high spin polarization [16, 17], which are crucial characteristics for magnetic recording and magnetoelectronic device applications. It is difficult to prepare CrO_2 at ambient pressure due to its metastable behavior, so CrO_2 powders (or thin films) are usually prepared through the

*Corresponding author: Tel: +86-13221019908
Fax: +86-28889526, e-mail: pzsi@cjlu.edu.cn

decomposition of CrO_3 instead of oxidation of Cr_2O_3 since the oxidation reaction generally proceeds extremely slowly [18-20]. Recently, Pei *et al.* obtained CrO_2 nanoparticles through the oxidation of $Cr(OH)_3{\cdot}1.1H_2O$ at 350 °C under 6 MPa of initial oxygen pressure [21]. In this work, the CrO_2 phase was prepared through the oxidation of laser ablated Cr_2O_3 nanoparticles under oxygen pressures of up to 40 MPa.

2. Experimental Details

The original Cr_2O_3 nanoparticles (Sample A) were prepared by exposing a piece of chromium metal in O_2 to a 20 W laser beam (Nd:YAG of 1064 nm) with subsequent drying in air at 353 K for 2 h. Sample A was then divided into three batches, and after that, the powders were annealed at 683 K in air for 1 h (Sample B) and in 40 MPa oxygen for 1 h (Sample C) and 4 h (Sample D). The high oxygen pressure was obtained by using a self-made high gas pressure heat-treatment apparatus. The structures of the samples were analyzed by using powder X-ray diffraction (XRD) with Cu *Kα* radiation. The morphology and the Cr/O ratio of Sample A was characterized using a Hitachi SU8010 scanning electron microscope (SEM) equipped with an energy dispersive spectrometer (EDS). The high-resolution lattices of the samples were observed with a Tecnai F20 transmission electron microscope (TEM). The magnetic hysteresis loops of the samples were then measured by using a Quantum-Design magnetic properties measurement system (Versalab-VSM) in fields of up to 2 T while the M-T curves were measured using a Lakeshore VSM.

3. Results and Discussion

As shown in Fig. 1(a), the x-ray diffraction patterns of Sample A could be indexed with Cr_2O_3. After 1 h of annealing at 683 K in air, the Cr_2O_3 phase does not change, and no other phases were detected in Sample B. However, the half-width of the diffraction peaks of the Cr_2O_3 in Sample B narrowed slightly, indicating the presence of Cr_2O_3 with a slightly enlarged crystalline size as a result of the heat-treatment. Moreover, a higher background was found in the x-ray diffraction patterns of sample A, indicating the presence of poorly crystallized particles with a very tiny grain size. The XRD patterns of both Sample C and D could be indexed with CrO_2 and Cr_2O_3. The presence of the CrO_2 phase indicates that the heat treatment with a high oxygen pressure was effective in preparing the meta-stable CrO_2. From a thermodynamic point of view, CrO_2 is more stable than Cr_2O_3 at

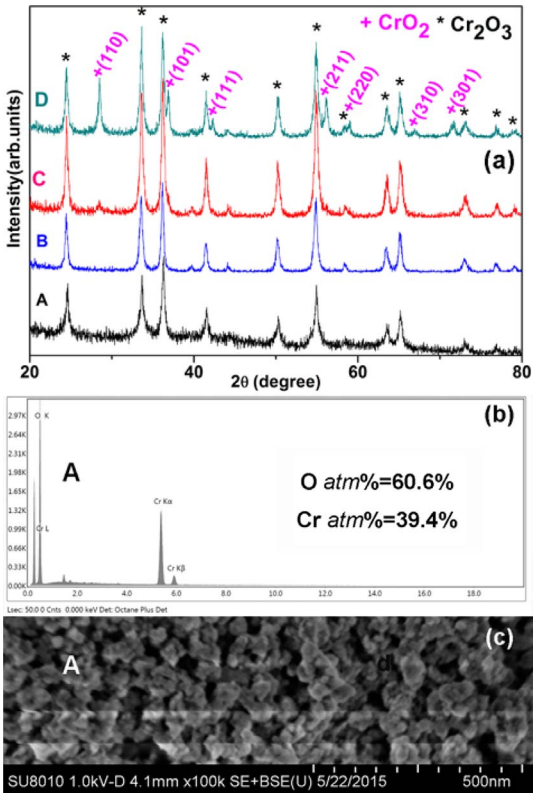

Fig. 1. (Color online) (a) X-ray diffraction patterns of the original Cr_2O_3 nanoparticles (Sample A) prepared via laser ablation and of the samples obtained after annealing Sample A in air (Sample B) and in 40 MPa oxygen for 1 h (Sample C) and 4 h (Sample D). * for Cr_2O_3 and + for CrO_2. (b) The EDS results of Sample A determined via SEM. (c) Morphology of Sample A observed via SEM.

683 K under 40 MPa of O_2, as shown in the pressure-temperature phase diagram of the Cr-O system [22]. Fig. 1(a) also shows that the relative intensity of the CrO_2 to Cr_2O_3 for sample D is much stronger than that for sample C, indicating that more CrO_2 was produced as the annealing time increased. The average crystalline size of the Cr_2O_3 in samples A, B, C, and D was estimated to be 20 nm, 26 nm, 22 nm, and 21 nm, respectively, according to the x-ray reflection peak width obtained by applying Scherrer's formula. The relatively larger crystalline size of sample B can be ascribed to the thorough crystallization of Cr_2O_3 under heat treatment in air. The medium crystalline size of Cr_2O_3 in Samples C and D is the joint result of the increase in size due to the heat treatment and the size reduction resulting from the formation of CrO_2. As shown in Fig. 1(b), the Cr/O elemental ratio of sample A, as measured by EDS, is very close to 1.5, which is in good agreement with that of the Cr_2O_3, as detected by the XRD. Fig. 1(c) shows the morphology of sample A, for

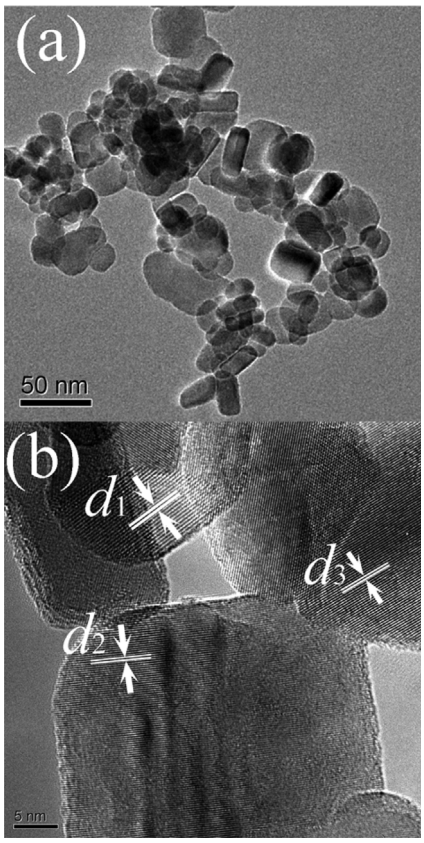

Fig. 2. TEM images of Sample B. The *d*-spacing of d_1 = 0.3655 nm, d_2 = 0.2422 nm, and d_3 = 0.2581 nm.

which most nanoparticles can be seen to have a size of less than 50 nm with a narrow size distribution.

Figure 2 shows the typical high-resolution images for Sample B. Most of the nanoparticles in Sample B are spherical or rectangular in shape, as shown in Fig. 2(a). The high-resolution images for sample B show that the nanoparticles are well-crystallized, as confirmed with the XRD results. The *d*-spacing of d_1 = 0.3655 nm, d_2 = 0.2422 nm, and d_3 = 0.2581 nm corresponds to the (012), (110), and (104) lattice spacing of Cr_2O_3, respectively, as shown in Fig. 2(b).

Fig. 3(a) shows the dependence of the magnetization curves on the temperature for sample D. A sharp magnetization drop was observed at 386 K, which is in good agreement with the Curie temperature for CrO_2. No changes in the magnetization were observed in the vicinity of the Néel temperature for Cr_2O_3. The magnetic hysteresis loops of Samples A, B, C, and D at 60 K and 300 K are shown in Fig. 3(b, c). The magnetization for Sample A shows a linear response to the applied magnetic field, and no magnetic hysteresis and zero coercivity were observed in Sample A. The magnetization for Sample B increases as the magnetic field increases and remains unsaturated at

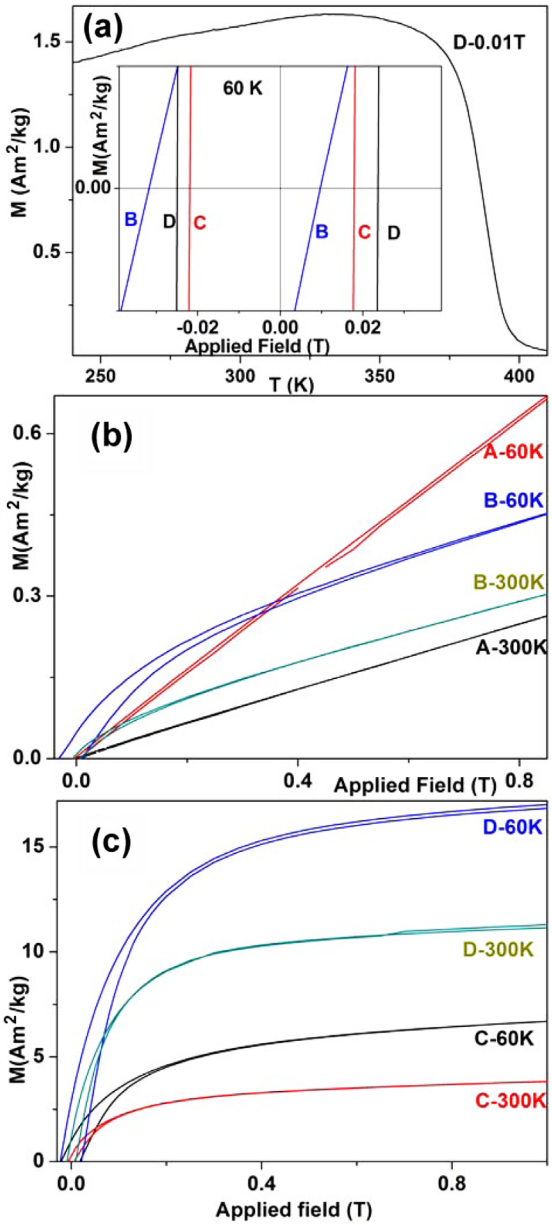

Fig. 3. (Color online) (a) The dependence on temperature of the magnetization of sample D. (b, c) Magnetic hysteresis loops for Samples A, B, C, and D at 60 K and 300 K. The inset of (a) shows the partially magnified M-H plots for Samples B, C, and D at 60 K.

2 T. The magnetization of Sample B at 2 T reaches 0.79 Am^2/kg at 60 K and 0.60 Am^2/kg at 300 K. An obvious loop shift was seen for sample B in the inset of Fig. 3(a). As mentioned above, Sample B is composed of Cr_2O_3 only, and bulk Cr_2O_3 is an antiferromagnetic material with a Néel temperature of 307 K. We therefore ascribe the weak ferromagnetic behavior of Sample B to the uncompensated surface spins. The exchange bias for Sample B at 60 K is ~11 mT, which originates from the exchange

coupling between the uncompensated surface spins and the antiferromagnetic core. The magnetization for Samples C (7.6 Am^2/kg at 2 T) and D (17.8 Am^2/kg at 2 T) at 60 K are much larger than those of Sample B (0.79 Am^2/kg at 2 T) due to the presence of CrO_2 in Samples C and D. The exchange bias in Sample C and D are 7 mT and zero, respectively, as shown in Fig. 3(a). It is interesting that the exchange bias decreases as the CrO_2 fraction increases, even though the samples were composed of AFM Cr_2O_3 and FM CrO_2. This phenomenon could be explained to be a result of the elimination of uncompensated spins originating from the Cr_2O_3 nanoparticle surface, over which most surface atoms transform into CrO_2 when exposed to high-pressure oxygen. It seems that the interfacial exchange interactions between the AFM Cr_2O_3 and the FM CrO_2 have a very limited effect on the exchange bias that decreases as the CrO_2 fraction increases. Usually, CrO_2 particles coated with a very thin Cr_2O_3 surface layer exhibit no exchange bias since the spins of the thin Cr_2O_3 layers are reversed with the applied field. However, thicker Cr_2O_3 layers could also result in an exchange bias [23]. We therefore speculate that the CrO_2 layers in our samples might be too thin for phase segregation, and thus they cannot dominate the exchange bias when competing with uncompensated surface spins. The CrO_2 phase might be segregated from the Cr_2O_3 nanoparticles since the melting point of CrO_2 is merely 648 K while that of Cr_2O_3 is 2708 K.

4. Conclusion

In summary, Cr_2O_3 and Cr_2O_3/CrO_2 nanoparticles were prepared by exposing a Cr metal piece in O_2 to a laser beam and subsequently annealing them under high-pressure oxygen at 40 MPa. The Cr_2O_3 nanoparticles are spherical or rectangular in shape with sizes ranging from 20-50 nm. A weak ferromagnetism and an exchange bias were observed as a result of the uncompensated surface spins in the Cr_2O_3 nanoparticles. The high oxygen pressure was effective in transforming the as-dried Cr_2O_3 nanoparticles to CrO_2, and the exchange bias in our Cr_2O_3/CrO_2 nanoparticles was dominated by the uncompensated surface spins over the Cr_2O_3 instead of by the interfacial exchange interaction between Cr_2O_3 and CrO_2.

Acknowledgements

We are grateful for the support from NSFC (Nos. 11074227, 51401198), Zhejiang Natural Science Foundation (LY14E010001), and China Postdoctoral Science Foundation (2014M560475).

References

[1] R. K. Gupta, E. Mitchell, J. Candler, P. K. Kahol, K. Ghosh, and L. Dong, Powder Technol. **254**, 78 (2014).
[2] S. B. Wang, K. Murata, T. Hayakawa, S. Hamakawa, and K. Suzuki, Catal. Lett. **63**, 59 (1999).
[3] Z. Pei and Y. Zhang, Mater. Lett. **62**, 504 (2008).
[4] W. S. Zhang, E. Brück, Z. D. Zhang, O. Tegus, W. F. Li, P. Z. Si, D. Y. Geng, and K. H. J. Buschow, Physica B **358**, 332 (2005).
[5] D. Vollath, D. V. Szabó, and J. O. Willis, Mater. Lett. **29**, 271 (1996).
[6] Z. C. Zhong, R. H. Cheng, J. Bosley, P. A. Dowben, and D. J. Sellmyer, Appl. Surf. Sci. **181**, 196 (2001).
[7] C. H. Lin, S. Y. Chen, N. J. Ho, D. Gan, and P. Shen, J. Phys. Chem. Solids **70**, 1505 (2009).
[8] Q. Z. Dong, J. D. Hu, Z. X. Guo, J. S. Lian, J. W. Chen, and B. Chen, Appl. Surf. Sci. **202**, 114 (2002).
[9] S. Khamlich, Z. Y. Nuru, A. Bello, M. Fabiane, J. K. Dangbegnon, N. Manyala, and M. Maaza, J. Alloys Compd. **637**, 219 (2015).
[10] N. Patel, A. Santini, V. Bello, G. Mattei, and A. Miotello, Surf. Coat. Technol. **235**, 784 (2013).
[11] M. Boutinguiza, B. Rodriguez-Gonzalez, J. del Val, R. Comesaña, F. Lusquiños, and J. Pou, Appl. Surf. Sci. **258**, 9484 (2012).
[12] C. C. Lin, C. J. Chen, and R. K. Chiang, J. Cryst. Growth **338**, 152 (2012).
[13] A. Tomou, D. Gournis, I. Panagiotopoulos, Y. Huang, G. C. Hadjipanayis, and B. J. Kooi, J. Appl. Phys. **99**, 123915 (2006).
[14] R. H. Kodama, S. A. Makhlouf, and A. E. Berkowitz, Phys. Rev. Lett. **97**, 1393 (1997).
[15] W. H. Meiklejohn and C. P. Bean, Phys. Rev. **102**, 1413 (1956).
[16] M. S. Anwar, M. Veldhorst, A. Brinkman, and J. Aarts, Appl. Phys. Lett. **100**, 052602 (2012).
[17] Y. Ji, G. J. Strijkers, F. Y. Yang, C. L. Chien, J. M. Byers, A. Anguelouch, Gang Xiao, and A. Gupta, Phys. Rev. Lett. **86**, 5585 (2001).
[18] Q. Zhao, Y. B. Fan, G. H. Wen, Z. G. Liu, H. A. Ma, X. P. Jia, G. T. Zou, and Ho-kwang Mao, Mater. Lett. **64**, 592 (2010).
[19] C. Aguilera, J. C. González, A. Borrás, D. Margineda, J. M. González, A. R. González-Elipe, and J. P. Espinós, Thin Solid Films **539**, 1 (2013).
[20] Y. Shibasaki, F. Kanamaru, and M. Koizumi, Mat. Res. Bull. **5**, 1051 (1970).
[21] Z. Pei, H. Xu, and Y. Zhang, Mater. Lett. **76**, 205 (2012).
[22] W. B. White and R. Roy, Geochim. Cosmochim. Acta **39**, 803 (1975).
[23] R. K. Zheng, H. Liu, Y. Wang, and X. X. Zhang, Appl. Phys. Lett. **84**, 702 (2004).